© 2017. Published by The Company of Biologists Ltd | Development (2017) 144, 3766-3776 doi:10.1242/dev.151761

RESEARCH ARTICLE

Cell migration, intercalation and growth regulate mammalian cochlear extension

Elizabeth Carroll Driver*, Amy Northrop and Matthew W. Kelley

ABSTRACT

Developmental remodeling of the sensory epithelium of the cochlea is required for the formation of an elongated, tonotopically organized auditory organ, but the cellular processes that mediate these events are largely unknown. We used both morphological assessments of cellular rearrangements and time-lapse imaging to visualize cochlear remodeling in mouse. Analysis of cell redistribution showed that the cochlea extends through a combination of radial intercalation and cell growth. Live imaging demonstrated that concomitant cellular intercalation results in a brief period of epithelial convergence, although subsequent changes in cell size lead to medial-lateral spreading. Supporting cells, which retain contact with the basement membrane, exhibit biased protrusive activity and directed movement along the axis of extension. By contrast, hair cells lose contact with the basement membrane, but contribute to continued outgrowth through increased cell size. Regulation of cellular protrusions, movement and intercalation within the cochlea all require myosin II. These results establish, for the first time, many of the cellular processes that drive the distribution of sensory cells along the tonotopic axis of the cochlea.

KEY WORDS: Inner ear, Cochlear development, Convergent extension, Radial intercalation, Live imaging, Mouse

INTRODUCTION

The cellular mosaic that comprises the mammalian auditory sensory epithelium – the organ of Corti (OC) – is a remarkable example of developmental patterning. Within the epithelium, hair cells (HCs) and associated supporting cells (SCs) are arranged into ordered rows that extend along the length of the tonotopic (base-to-apex) axis. Although the functional relevance of this cellular pattern has not been directly demonstrated, its emergence correlates with the appearance of an elongated cochlear duct, which represents a crucial step in the evolution of precise frequency discrimination. The mosaic of HCs and SCs combines with functional gradients in basilar membrane mechanics and anatomy to create a tonotopic array in which different frequencies stimulate HCs at different positions along the cochlear base-to-apex axis (Mann and Kelley, 2011). Auditory sensory epithelia in reptiles and other poikilothermic vertebrates are generally round or ovoid in shape, suggesting that considerable developmental remodeling must occur to produce the extended sensory epithelium observed in mammals. However, the factors that regulate this process are largely unknown.

Laboratory of Cochlear Development, National Institute on Deafness and Other Communication Disorders, NIH, Bethesda, MD 20892, USA.

*Author for correspondence (drivere@nidcd.nih.gov)

E.C.D., 0000-0002-5618-1053

Received 14 March 2017; Accepted 24 August 2017

The cochlear duct develops as an out-pocketing arising from the ventral region of the otocyst beginning around embryonic day (E) 11 in the mouse, but does not reach its mature length (~6 mm) until the postnatal period (Burda and Branis, 1988; Mu et al., 1997; Ou et al., 2000). Although the epithelial cells of the duct appear largely homogenous at early time points (McKenzie et al., 2004), multiple structures, including the OC, will develop from cells located in specific regions. Considering the diversity of cellular phenotypes that will develop within the duct, the relative contributions of cell growth, proliferation and migration may vary between regions. Of particular interest are the progenitor cells [referred to as prosensory cells (PrCs)] that will give rise to all of the HCs and SCs within the OC. The entire population of PrCs becomes postmitotic by E14 (Chen and Segil, 1999; Ruben, 1967). However, at E14, the duct is typically less than 3 mm in length (McKenzie et al., 2004). Therefore, for the OC to extend along the full length of the tonotopic axis, the PrC population must be redistributed as the cochlear duct grows.

Following terminal mitosis, PrCs are arranged as a band of pseudostratified cells within the floor of the duct. Morphometric analyses of the changes of distribution of these cells in fixed tissues suggested a progressive extension along the base-to-apex axis of the cochlea along with a concomitant thinning of the epithelium (Chacon-Heszele et al., 2012; Chen et al., 2002; McKenzie et al., 2004). These changes are consistent with radial intercalation (RI) of PrCs along the axis between the basement membrane and the luminal surface (basal-luminal) (Chen et al., 2002; Ossipova et al., 2015). Further, analysis of cochleae from different planar cell polarity (PCP) mouse models have indicated shortened cochleae and defects in cellular patterning (Montcouquiol et al., 2003; Wang et al., 2006, 2005). Based on these results, it has been suggested that cochlear elongation and cellular patterning may also be regulated through a developmentally conserved process known as convergence and extension (CE). During CE, cells within a plane rearrange from a shorter and wider domain to one that is longer and narrower (for a review, see Tada and Heisenberg, 2012). This occurs as cells located orthogonal to the axis of extension actively migrate towards the midline, where they intercalate with other midline cells, leading to subsequent extension. Although changes in the spatial distribution of PrCs are consistent with both CE and RI, direct evidence has never been demonstrated. We sought to examine the cellular processes that mediate cochlear outgrowth using a combination of morphometric analyses and time-lapse imaging.

RESULTS

RI and cell growth occur during formation of the OC

PrCs were visualized in whole-mount preparations of cochlear ducts from E14, E16 and postnatal day (P) 0 by double labeling with anti-CDKN1B [$p27^{kip1}$ (Chen and Segil, 1999)] and anti-SOX2 (Kiernan et al., 2005) (Fig. 1). The physical distribution of PrCs and epithelial volume were determined for a 100 µm segment

DEVELOPMENT

Development (2017) 144, 3766-3776 doi:10.1242/dev.151761

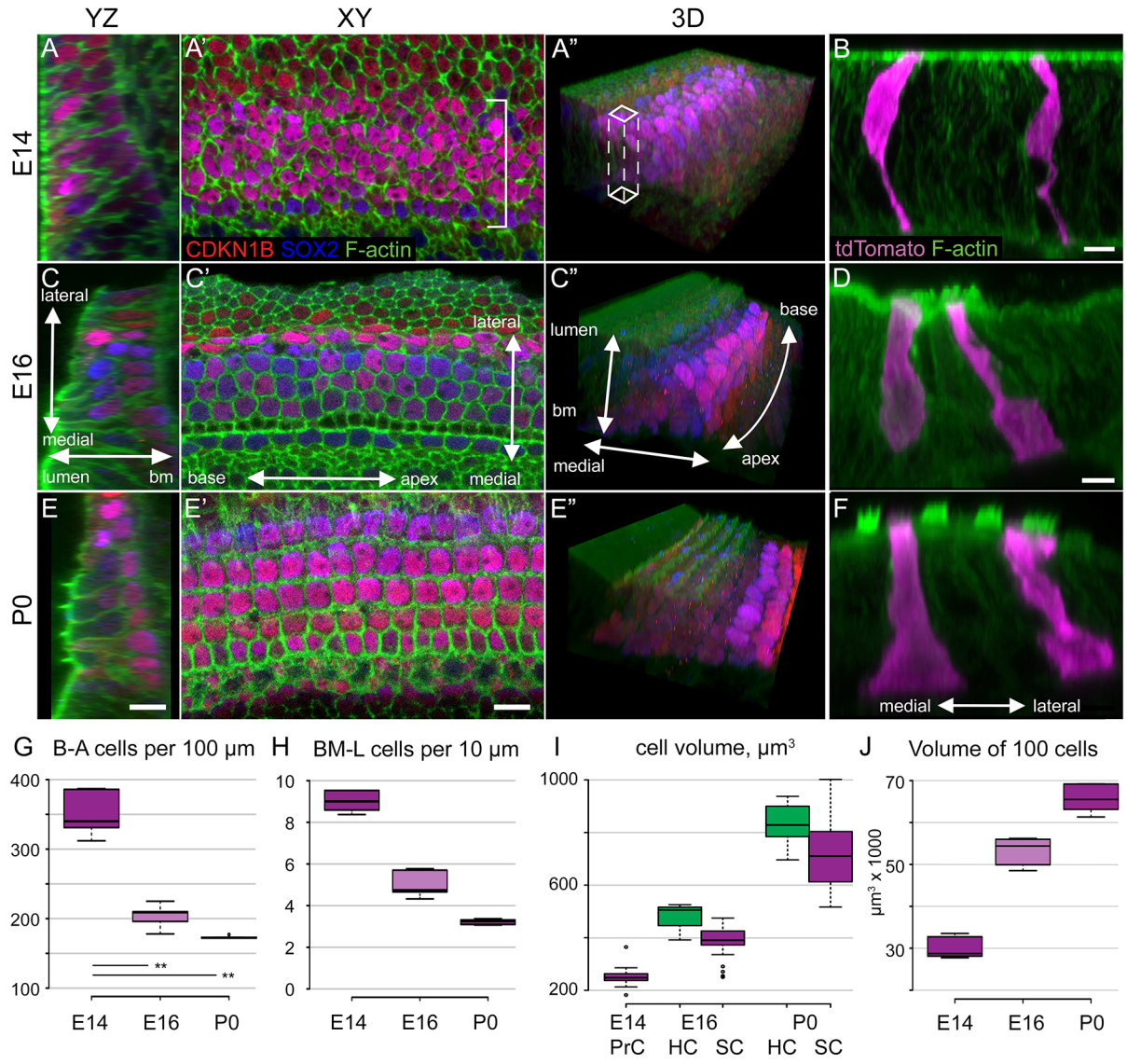

Fig. 1. Extension of the cochlear duct. (A,C,E) Single-plane confocal images of the base of the mouse cochlear duct at the indicated time points and orientations, with axes shown in C,C′ (bm, basement membrane). 3D renderings are shown in A″,C″,E″. PrCs and their derivatives, namely HCs and SCs, are marked with anti-CDKN1B (red) and anti-SOX2 (blue), together with F-actin (green). Scale bars: 10 µm. (B,D,F) *yz* optical projections of *Sox2*^{CreERT2}*; R26R*^{tdTomato} cochleae with tdTomato-filled PrCs, HCs and SCs (magenta) and F-actin (green). Scale bars: 5 µm. (A-A″) At E14, PrCs are grouped in a pseudostratified band. (B) E14 PrCs have morphologies consistent with undifferentiated, pseudostratified epithelial cells. (C-D) At E16, the basal region of the cochlear duct has developed the basic cellular pattern of the OC, with rows of developing inner and outer HCs evident. (E-F) At P0, differentiation of the OC is evident and HCs have developed stereociliary bundles. Distinct SC phenotypes, such as pillar cells and Deiters' cells, can be identified based on tdTomato labeling. (G) Quantification of cell number within a section of the epithelium extending along 100 µm of the axis of extension [base-to-apex (B-A)] indicates a significant decrease of ~42% between E14 and E16 (P<0.01). By contrast, the decrease between E16 and P0 is only 15% (not significant). n=5 samples for each age. (H) To quantify cellular stratification, the number of cells within a 10×10 µm column extending between the basement membrane and the luminal surface (BM-L, A″) was determined for each time point. Stratification significantly decreases from an average of 9.33 cells at E14 to 5.04 cells at E16 and 3.21 cells at P0. P<0.01 for all pairwise comparisons; n=5. (I) As PrCs develop into HCs or SCs, there are significant increases in cell volume. Number of cells: E14, 19; E16, 13 HCs, 40 SCs; P0, 6 HCs, 23 SCs. P<0.01 for all comparisons except P0 HCs versus SCs, P<0.05. (J) To illustrate the effects of changes in cell volume on cochlear extension and growth, the epithelial volume of 100 PrCs and/or their derivatives was determined at each time point. Results indicate significant increases (P<0.01; n=5) between each time point, demonstrating that cell growth contributes to cochlear extension.

extending along the base-to-apex axis in the basal region of the cochlear duct. At E14, a median value of 340 PrCs per 100 µm are arranged as a dense, pseudostratified band (Fig. 1A,G). To quantify radial stratification, we calculated the average number of cells in a 10×10 µm column extending along the basal-luminal axis (Fig. 1A″,H). At E14, such a column would contain on average 9.31 cells. At E16, the median number of PrCs per 100 µm segment is 225.0, and the number of cells per 10×10 µm column is 5.5 (Fig. 1C,G,H). Both of these values are significantly reduced by comparison with E14 (P<0.01), indicating a significant decrease in radial stratification that is consistent with RI. At P0, average cell density per 100 µm segment is 173.2, a slight decrease from E16 [not significant (n.s.)], and radial stratification has decreased to 3.21 cells per 10×10 µm column (P<0.01) (Fig. 1E,G,H).

To determine whether changes in cell size also play a role in extension of the OC, a low level of *Sox2*^{CreERT2} (Arnold et al., 2011)

Development (2017) 144, 3766-3776 doi:10.1242/dev.151761

activity was induced to achieve sparse cellular labeling with the *R26R*^{tdTomato} reporter (Madisen et al., 2010), and we measured PrC, HC and SC shape and volume at the same developmental time points (Fig. 1B,D,F). Relative to E14, HCs and SCs at E16 show a significant increase in volume, which is even greater at P0 (Fig. 1I). Next, the epithelial volume of a group of 100 contiguous PrCs or HCs and SCs was calculated at each time point (Fig. 1J). Between E14 and E16, the epithelial volume for 100 PrCs is significantly increased (P<0.01), consistent with increased PrC cell volume. Analysis of changes along the medial-lateral (width), base-to-apex (length) and basal-luminal (thickness) axes indicated that this increase is primarily driven by spreading of these cells along the base-to-apex axis, as the thickness and width of the epithelium were unchanged between E14 and E16 (Fig. S1). Later, between E16 and P0, epithelial volume for a contiguous population of 100 PrC derivatives (HCs and SCs) also significantly increased, despite concomitant epithelial thinning, due to an increase in both length and width. Since cellular stratification decreases between E16 and P0, these results suggest that widening and lengthening of the epithelium between these time points occurs as a result of increased cellular volume.

Overall, these results suggest that cochlear outgrowth between E14 and E16 is a result of RI, leading to cellular movement towards the apex and increased cell size. By contrast, between E16 and P0, although a small amount of RI still occurs, increased cell size appears to be the primary mechanism for continued cochlear extension.

OC cells move toward the cochlear apex during development

To directly visualize the movements of PrCs and their derivatives during extension, mice carrying an inducible *Atoh1*^{Cre*PR} allele (Rose et al., 2009) were crossed with either the *R26R*^{tdTomato} or *R26R*^{ZsGreen} reporter line (Madisen et al., 2010). Cochlear explants were established at E13 or E14, and transected in the mid-apex to promote extension (Wang et al., 2005). A low level of Cre activity was induced to fluorescently label a sparse number of PrCs or their derivatives (Driver et al., 2013) and we then generated time-lapse movies initiated at the equivalent of E14 or later, and tracked individual cell movements (Fig. 2A, Movie 1). Because cochlear development occurs in a gradient from base to apex, images were obtained at two positions within explants, one near the base and one near the cut edge (Fig. 2B, Movie 2). The movements of cells located in the mid-apex at E15 were strongly biased towards the apex of the duct, but some changes in position along the orthogonal medial-lateral axis were also observed, along with some medial-lateral movement of the entire epithelium. By contrast, cells located in the more mature basal region of the epithelium showed less movement (arrows, Fig. 2B′). Rates of cellular displacement were much greater for mid-apical cells in comparison to cells located in the base, and the straightness index (a measure of directed migration) was significantly higher (Fig. 2C,D).

To determine whether the rate of cellular extension changes over developmental time, the displacement of mid-apical OC cells was determined in time-lapse movies initiated at the equivalent of E14 to E18. Cell displacement rates were fastest at E14 (10 µm/h, which is slightly more than one cell diameter per hour; Fig. 2E), roughly the same from E15 to E16, and slowed by E17. To confirm that imaging conditions did not influence cellular migration, explants were cultured on gridded coverslips, and images of the mid-apical region were obtained every 24 h over 5 days *in vitro* (DIV) (Fig. 2F). The movement of cells measured in this manner is similar to that observed in the time-lapse images: 150 µm-250 µm per day, equivalent to ∼6-11 µm/h. The rate of movement of cells in time-lapse movies is also roughly comparable to the overall growth of the cochlea *in vivo*, at ∼11 µm/h between E14.5 and P0, with the highest rate of growth being between E16 and E17 (McKenzie et al., 2004), indicating that our time-lapse imaging provides an accurate representation of this developmental process in the cochlea.

OC cells extend and converge relative to one another

The overall rate of extension described above is a result of multiple ongoing processes, including cellular intercalation, either through RI, CE or both, collective cellular migration, and increasing cell size. To estimate the relative contribution of cellular intercalations between existing cells, we identified nearby pairs of cells in the mid-apex and determined relative changes in distance between those cells along both the x (extension, base-to-apex) and y (convergence, medial-lateral) axes during the middle 6 h of time-lapse movies initiated on the equivalent of E14, E15, E16 or E17 (Fig. 3A,B, Movie 3).

Although several mechanisms can account for a change in the relative distance between two cells, one of the primary mechanisms is likely to be intercalation of other cells in the intervening region. At E14 and E15, the distance between cells along the y-axis decreased (ΔY), whereas the distance along the x-axis increased (ΔX) (Fig. 3C). The positive change along the x-axis and the negative change along the y-axis are consistent with CE. However, because these measurements were performed on projections of all z-planes, it was not possible to similarly examine possible effects of RI. The rate of change of PrCs relative to one another on E14 or E15 was ∼3.5 µm/6 h. This was far less than the overall extension of individual cells illustrated in Fig. 2; however, it is important to consider that the overall extension represents not only the migration of the cells being analyzed, but also the contribution to extension from the outgrowth of all the cells located more basally. To estimate the contribution of changes in relative distance between two cells versus ongoing collective migration, we partitioned the entire epithelium into 25 µm bins, based on the average distance between the cells that were analyzed for changes in relative position. We estimated the average length of the entire cochlear duct to be 1500 µm at the beginning of an experiment, and then divided the 250 µm growth per day into 60-25 µm bins. Based on this calculation, the collective migration within a single 25 µm bin is ∼4 µm per day. However, within that same 25 µm bin the cell located more apically travels an additional 14 µm (3.5 µm per 6 h, Fig. 3C) for a total movement of 18 µm. Of that 18 µm, 14 µm are attributable to differential cell movement, suggesting that up to 77% of cell movement on E14 or E15 is a result of cellular intercalation.

At E16 and E17, rates for both ΔX and ΔY decreased significantly, with ΔY essentially dropping to zero (Fig. 3C). As the cochlea is continuing to grow at these ages (McKenzie et al., 2004; Yamamoto et al., 2009), the cellular movements that occur (Fig. 1E) are probably minimally influenced by RI or CE but, as discussed above, are a result of increasing cell volume and collective migration (Fig. S1).

Previous work has demonstrated that cellular intercalation – the movement of one or more cells in between two other cells – plays a key role in driving RI and CE. One morphological indicator of ongoing intercalation is the presence of luminal cell-cell junctions that include more than three cells (Bertet et al., 2004; Blankenship et al., 2006). We mapped the geometry of cell-cell junctions within the prosensory domain at different developmental stages. At E14, almost half of all cell-cell junctions within the sensory epithelium include more than three cells (Fig. 3F-H). However, by E16, the percentage of junctions in the lateral OC that include more than

Development (2017) 144, 3766-3776 doi:10.1242/dev.151761

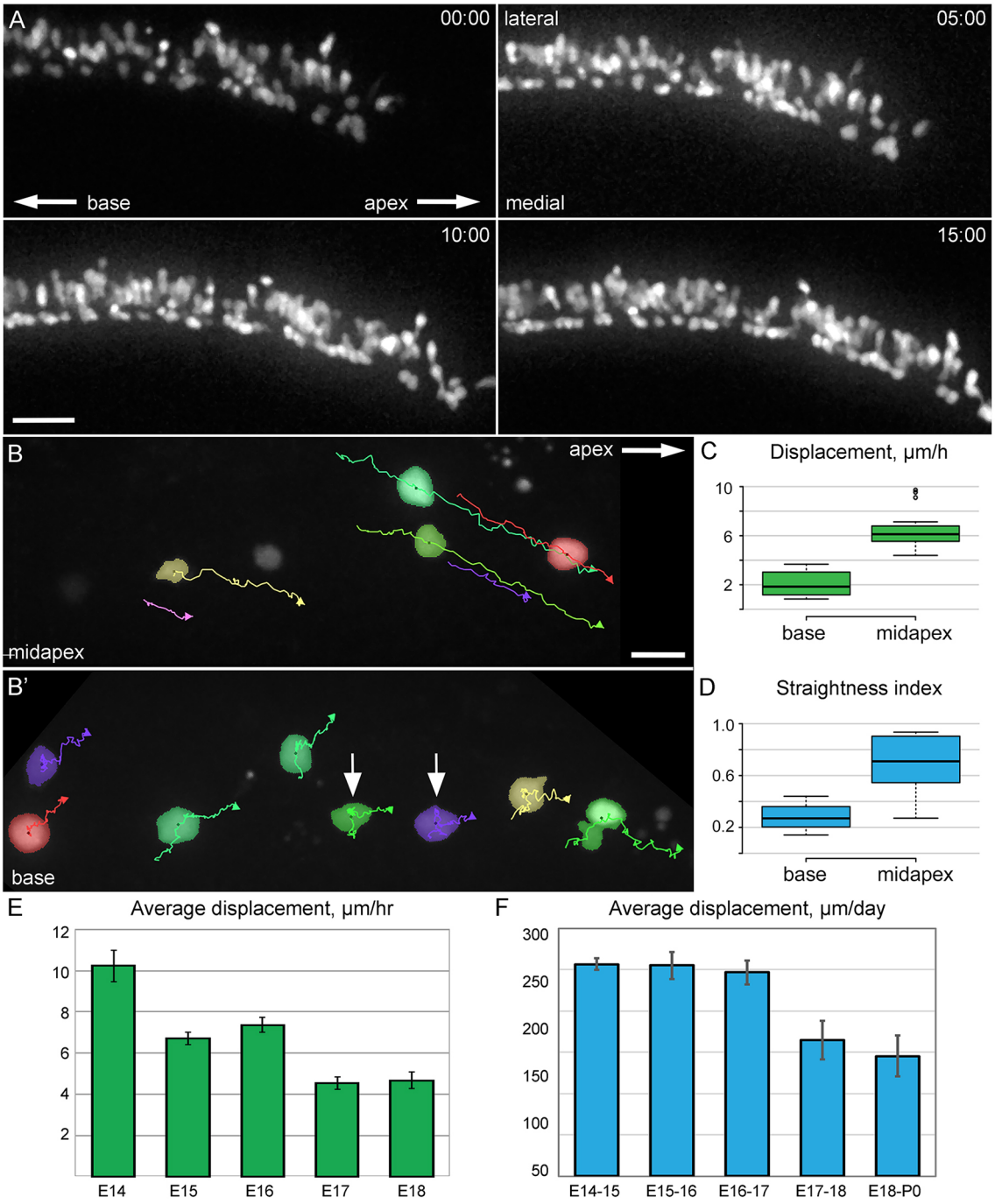

Fig. 2. OC cells migrate towards the cochlear apex. (A) *z*-stack projection images from an *Atoh1*^{Cre*PR}; *R26R*^{tdTomato} cochlear explant established at E13 and imaged at 2 DIV (E15 equivalent). Indicated time points (h:min) are relative to the beginning of the time-lapse. Lengthening and slight narrowing of the population of labeled cells are apparent as they move in the apical direction. Scale bar: 50 μm. (B) Migration tracks for pseudocolored individual cells from an *Atoh1*^{Cre*PR}; *R26R*^{ZsGreen} 16 h time-lapse video started at 1 DIV (E14). A single explant was imaged near the mid-apex (B) and at the base (B′) of the cochlea. Cells at the mid-apex move steadily in the apical direction; cells at the base show less consistent migratory paths. Some cells are nearly stationary (arrows). Scale bar: 20 μm. (C) Displacement rates (μm/h) for individual cells located at the mid-apex are significantly greater than those at the base (P<0.001). (D) Average straightness index of cells at apex versus base, indicating that cells in the mid-apex migrate in a straighter line (P<0.001). (C,D) n=3 explants, 18 cells. (E) Average displacement of migrating cells on the indicated embryonic day equivalents, taken from time-lapse sequences of 10-16 h. The rate of cell movement gradually decreases with developmental age. All differences are statistically significant (P<0.01), except E14 versus E16, and E15 versus E16. n=(age, explants, cells): E14, 7, 41; E15, 9, 68; E16, 8, 75; E17, 10, 66; E18, 6, 30. (F) Average displacement of cells per day when imaged once every 24 h. Early (E14-E16) values are all significantly different (P<0.01) from late (E17-P0) values. n=(age, explants, cells): E14, 4, 14; E15, 5, 15; E16, 7, 24; E17, 4, 14; E18, 4, 14. (E,F) Data shown are averages±s.e.m.

three cells is less than 30%, and at P0 is ∼10% (Fig. 3H). These results are consistent with the observation that RI and CE are significantly decreased after E16. Some four-cell junctions do persist at this stage, possibly as a result of ongoing refinement of the cellular pattern of the OC, which is incomplete by E16 (Fig. 3J-L, see below).

Development (2017) 144, 3766-3776 doi:10.1242/dev.151761

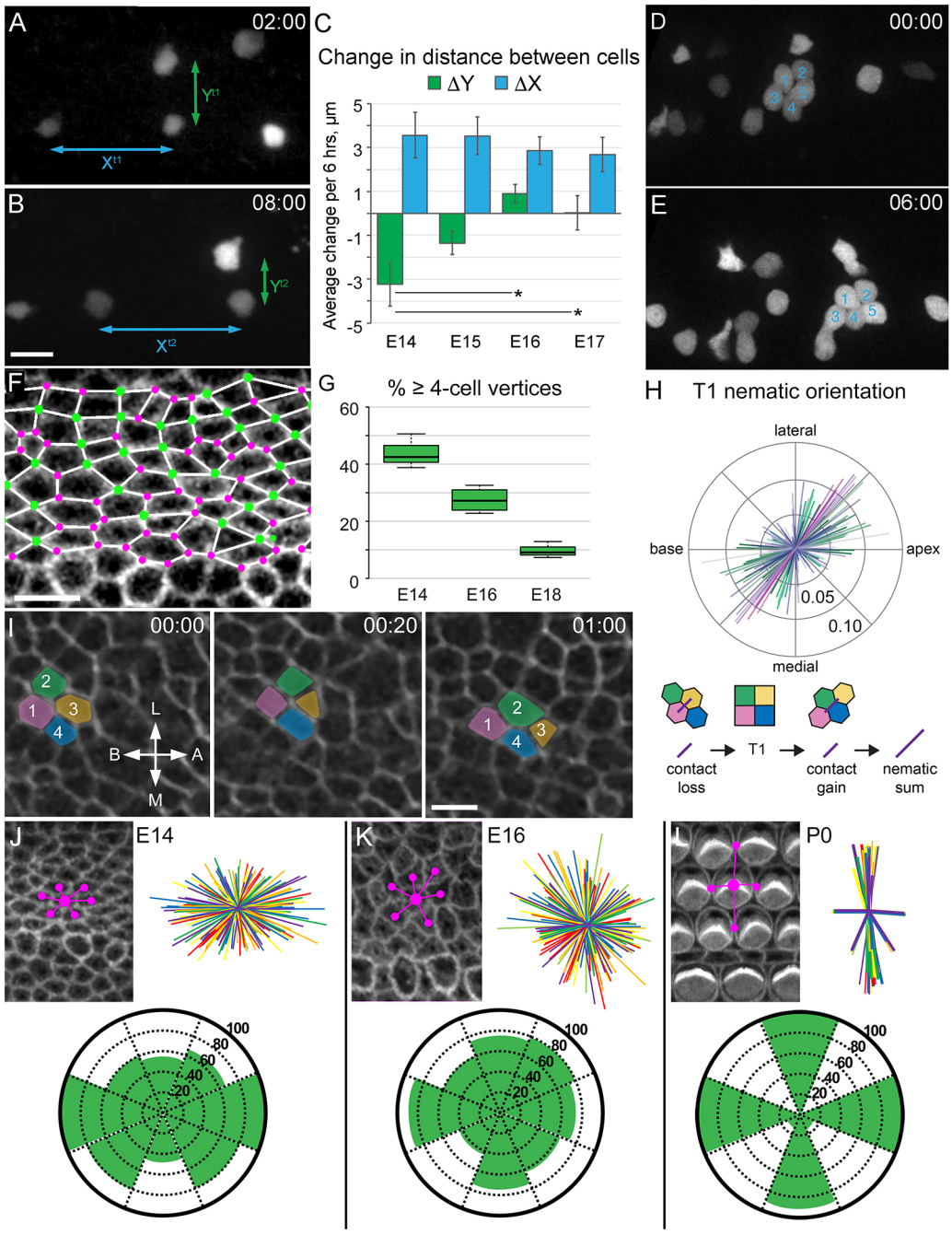

Fig. 3. CE occurs during cochlear outgrowth. (A,B) *z*-stack projections from an *Atoh1*^{Cre*PR}; *R26R*^{ZsGreen} time-lapse begun at E14 equivalent, showing CE measurements. The distance between cells along the *x*-axis (base-to-apex) increases, whereas distance along the *y*-axis (medial-lateral) decreases. Scale bar: 20 µm in B for A,D,E. (C) Quantification of average change in distance between nearby pairs of cells over 6 h. Convergence (negative ΔY) and extension (positive ΔX) are observed at E14-E15. Extension continues until E17, but little convergence is observed beyond E15. Data shown are averages±s.e.m., and statistically different values are indicated (P<0.01). *n*=(age, explants, cell pairs): E14, 8, 26; E15, 8, 28; E16, 5, 46; E17, 5, 45. (D,E) Cells align into rows in an E15 *Atoh1*^{Cre*PR}; *R26R*^{tdTomato} cochlear explant. A rosette of labeled HCs (D, numbered) rearranges into the first and second rows of OHCs over 6 h (E). (F) The luminal surface of a phalloidin-stained E14 cochlear epithelium, overlaid with depictions of the cell vertices. Vertices of three cells are marked with a pink dot, and those containing four or more cells with a green dot. Scale bar: 5 µm. (G) The percentage of cell vertices containing four or more cells decreases with developmental age. Values are significantly different (P<0.01). *n*=(age, sample, cell vertices): E14, 3, 740; E16, 4, 1170; E18, 3, 657. (H) The orientation of T1 transition summed nematics at E15, with axes indicated. Each line represents the average orientation of four-cell (T1) vertices resulting in neighbor exchange in a single time-lapse frame. The lengths of the lines along the nematic norm reflect how uniformly ordered the orientations of the exchanges are. A horizontal line orientation indicates productive neighbor exchange leading to extension along the base-to-apex axis, but the majority of the T1 nematics are oriented at ~45°, between the base-to-apex and medial-lateral axes. Productive T1 neighbor exchange and summed nematic is depicted below the plot. *n*=3 explants, 143 frames, 1238 cells. (I) Still images of a 2 µm luminal surface *z*-stack confocal projection from an E14 *R26R*$^{mT-mG}$ cochlear explant, with four cells pseudocolored and numbered. In 1 h, cells 2 and 4 intercalate between cells 1 and 3. A common vertex forms, then resolves as cells 2 and 4 intercalate perpendicular to the base-to-apex elongation axis. Scale bar: 5 µm. (J-L) Luminal surface views of the OC at the indicated ages. Spatial relationships for cell-cell contacts were determined as shown (magenta lines). An overlay of spatial relationships for multiple cells in the OHC region is shown for each age. Orientations of cell-cell contacts at E14 and E16 are similar. At P0 cellular patterning has changed significantly. Rose diagrams illustrate the percentage of cells with contacts at the indicated positions. *n*=(age, samples, cells, contacts) E14, 3, 45, 271; E16, 3, 45, 179; P0, 3, 45, 123.

Development (2017) 144, 3766-3776 doi:10.1242/dev.151761

To assess intercalation more closely, we examined time-lapse videos from samples in which a group of labeled cells were clustered together. As illustrated in Fig. 3D,E, at time 0:00, the five indicated cells (most likely HCs) are arranged in a rosette (presumably separated by unlabeled SCs); by time 6:00, cell 4 has intercalated between cells 3 and 5 (see Movie 4). To directly visualize examples of intercalation, extension assays were established from *R26R*$^{mT\text{-}mG}$ mice, which express membrane-targeted tdTomato in all cells (Muzumdar et al., 2007). An example of a T1 neighbor exchange in the prosensory region is shown in Fig. 3I (see also Fig. S2). However, since four-cell vertices can form and subsequently resolve without neighbor exchange, we quantified the orientation of T1 transitions resulting in neighbor exchange in three E15 *R26R*$^{mT\text{-}mG}$ explants using the TissueMiner software package (Etournay et al., 2016). Basic analysis of the cell rearrangements indicated that most cellular intercalations are oriented at a ∼45° angle between the base-to-apex and medial-lateral axes (Fig. 3H). This orientation would be likely to lead to expansion of the tissue both towards the apex and mediolaterally, which may be influenced by the tendency of the sensory epithelium to spiral, even in explant culture.

Cellular patterning is incomplete at the end of CE

An unexpected observation from these experiments was that although cochlear extension continues for several more days, relative cell rearrangements are significantly decreased by E16 (Fig. 3C). As described above, extension beyond this age is likely to be mediated through individual cell growth. If relative cell movements play a role in cellular patterning, then these results suggest that the basic pattern of the OC should be complete by E16. To examine this, the geometric organization of cells within the mid-apical outer hair cell (OHC) region was examined at E14 (before HC differentiation), E16 (onset of HC differentiation) and P0 (mature pattern). At each stage, we determined the orientation of neighboring cells around randomly selected individual PrCs (E14) or HCs (E16, P0) (Fig. 3J-L). At E14 and E16, cell-cell contacts were nearly uniformly distributed around each single cell. By contrast, at P0, cell-cell contacts were almost entirely restricted to the base-to-apex and medial-lateral axes of the OC. These results suggest that as RI and CE cease at ∼E16, cells have been redistributed along the long axis of the cochlear duct, but the unique cellular pattern of the OC has not yet developed.

PrCs/SCs extend dynamic protrusions along the basement membrane

Characterizations of migrating cells in other epithelia have demonstrated the generation of cellular protrusions that are biased towards the direction of cell movement (Elul and Keller, 2000). To further examine the protrusive activity of PrCs, HCs and SCs between E14 and E16, we used *Sox2*^{CreERT2} (Arnold et al., 2011) to increase the proportion of labeled PrCs/SCs, and the membrane-associated EGFP expressed by the *R26R*$^{mT\text{-}mG}$ reporter (Muzumdar et al., 2007) to image cellular boundaries. In orthogonal (*xz*) views of time-lapse images, two cellular morphologies were present: long progenitor-like cells spanning the epithelium (PrCs and immature SCs), and luminal flask-shaped cells that extended approximately halfway to the basement membrane (immature HCs) (Driver et al., 2013; Kiernan, 2013). Analysis of both *xy* (surface) and *xz* views of PrCs/SCs indicated that these cells are actively migrating, and that they extend and retract multiple cellular protrusions along their lateral surfaces, with many extending along the basement membrane (Fig. 4A,B, arrows, Movie 5). By contrast, HCs extend limited cellular protrusions (Fig. 4A,B). Using CellGeo (Tsygankov et al., 2014), we defined and tracked cellular protrusions at E15, and quantified the relative difference in protrusive activity of PrCs/SCs versus HCs over time (Fig. 4C). The protrusions of PrCs/SCs persisted longer on average than those of HCs, and individual PrCs/SCs averaged more than twice as many protrusions per cell per frame compared with HCs (Fig. 4D). These data suggest that PrCs/SCs, which are the cells primarily in contact with the basement membrane at these stages, might act as the driving force for migratory extension within the OC.

In other tissues undergoing CE, cellular protrusions are primarily oriented along the axis of convergence, perpendicular to the axis of extension (Voiculescu et al., 2007; Wallingford et al., 2000; Williams et al., 2014). If CE plays a major role in cochlear extension and the protrusions of PrCs/SCs are important for this process, then we expected to see a protrusive bias along the medial-lateral axis. Therefore, we measured the angles of protrusions relative to the centroids of the cells at time points between E14 and E16 (Fig. 4E). At E14, all PrCs/SCs were grouped together. The protrusions of the PrCs were biased along the medial-lateral axis, particularly toward the medial side. At E15, an overall bias in the orientation of protrusions was still present in PrCs/SCs, but the predominant orientation was ∼45° relative to both the medial-lateral and base-to-apex axes. This orientation is consistent with the observed 45° angle of the T1 nematics (Fig. 3H), since the direction of cellular protrusions during convergence is usually perpendicular to the axis of extension. To determine if the distribution of protrusions was affected by the position of SCs within the OC, we analyzed E15 medial SCs and lateral SCs separately. This analysis did indicate a difference in the distribution of protrusions, with both cell populations exhibiting more processes oriented towards the pillar cells, which separate the inner (medial) and outer (lateral) rows of HCs and SCs at the midline of the sensory epithelium (P<0.005). However, for both populations, the axis of orientation was approximately mid-way between the axis of extension and the perpendicular medial-lateral axis. By E16, when convergence, but not extension, has ended, the distribution of protrusions of SCs is unbiased, even though the number of protrusions per SC is unchanged by comparison with E14 or E15. Lateral protrusions generated by E15 and E16 HCs show a bias towards the medial side (P<0.005) but, as these cells are not in contact with the basement membrane, it is still unclear what role these HC extensions might play.

To confirm that protrusive activity also occurs *in vivo*, we used a low level of *Sox2*^{CreERT2} induction to label developing PrCs/SCs *in vivo*, and fixed samples at E15. Numerous protrusions were observed on both SCs and HCs (Fig. S3).

Myosin II activity is required for cochlear cell migration and intercalation

Previous results have demonstrated that the three non-muscle myosin II (MyoII) heavy chains (MYH9, MYH10 and MYH14) are expressed in unique patterns within the cochlear duct (Yamamoto et al., 2009). In particular, MYH9 and MYH10 are expressed in PrCs and developing HCs and SCs. Moreover, MyoII activity is required for cochlear outgrowth (Yamamoto et al., 2009). To determine the overall role of MyoII in migrating PrCs/SCs, the behaviors of individual cells were imaged in explants exposed to the MyoII inhibitor blebbistatin at E15 (Fig. 5A-C). Blebbistatin treatment inhibited cell movement and induced a loss in the bias of protrusions in the direction of migration (Fig. 5A-C, Movies 6, 7; data not shown). In addition, blebbistatin caused up to 85% of developing HCs to fully re-extend a basal process, like that of immature HCs, demonstrating that retraction of this protrusion is MyoII dependent, but did not affect HC differentiation

Development (2017) 144, 3766-3776 doi:10.1242/dev.151761

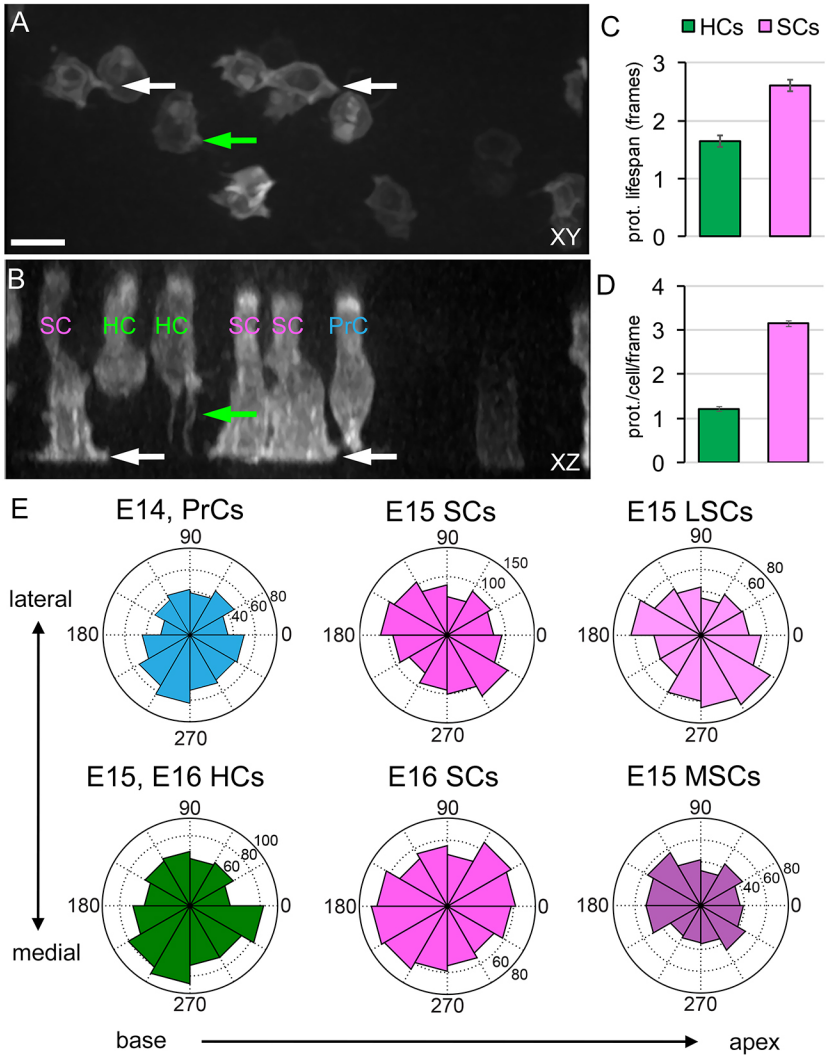

Fig. 4. Migrating cochlear epithelial cells generate cellular protrusions. (A,B) Images from a *Sox2*^{CreERT2};*R26R*$^{mT\text{-}mG}$ E15 explant, labeled with membrane EGFP. (A) *xy* (luminal) view; (B) *xz* (luminal-basal) view. Cellular protrusions are present on both SCs and HCs. SC protrusions extend primarily along the basement membrane (white arrows). HCs generate thin basal projections (green arrows). Putative cell types are labeled in B. Scale bar: 10 µm. See Movie 5. (C) Duration of cellular protrusions in HCs and SCs. The average lifespan of an SC protrusion is longer than that of a similar protrusion in an HC (P<0.001). (D) SCs display nearly three times as many protrusions over time than HCs (P<0.001). (C,D) n=5 explants, 23 cells, 1365 protrusions, 1261 frames (1 cell/frame). (E) Distribution of angles of protrusions in *xy*, relative to cell centroid, in the indicated cell types at the indicated time points. Analysis of protrusions in PrCs at E14 indicates a non-uniform distribution (P<0.05), with a bias towards the medial side of the epithelium. At E15, SC protrusions also show a non-uniform distribution (P<0.005), skewed 45° towards the axis of extension. Separation of E15 SCs based on position within the developing OC [lateral supporting cells (LSCs) are in the OHC region and medial supporting cells (MSCs) are in the inner hair cell (IHC) region] indicates that the distributions differ (P<0.005), with more protrusions in each region towards the midline. At E16, no bias in the distribution of protrusions was observed in SCs. E15 or E16 HCs did show a bias in protrusions towards the medial side (P<0.005), but these cells do not contact the basement membrane. n=(age, cells, protrusions): E14, 13, 537; E15, 23, 1365; E16, 16, 1239.

(Fig. S4, Movie 8). Following washout, cells resumed migratory activity. Inhibition of MyoII also led to a rapid increase in the luminal surface area of developing SCs, and to a decrease in the height of cells between the basement membrane and the luminal surface (Fig. 5A,D, E, Movie 6). This caused an increase in distance between developing HCs, and a general relaxation of the entire sensory epithelium (Fig. 5B, Movie 7), as in previous observations of neonatal cochlear explants (Ebrahim et al., 2013).

MyoII has been shown to play a role in cellular intercalation (Bertet et al., 2004; Rozbicki et al., 2015). To determine whether MyoII activity is required for cellular intercalation during cochlear elongation, the number of cell-cell junctions containing four or more cells was examined in cochlear explants following 2 days of blebbistatin treatment beginning at E14 (Fig. 5F,G). Results indicated a significant decrease in the number of cell-cell junctions between four or more cells, suggesting fewer intercalation events (Fig. 5H). This prolonged exposure to blebbistatin led to significant increases in the luminal surface area of all cell types (Fig. 5I), demonstrating multiple roles for MyoII in cell morphology, migration and intercalation.

DISCUSSION

The evolution of an elongated, tonotopically organized auditory organ is a key step in the ability of mammals to discriminate frequencies. A crucial aspect of the development of such a structure is the remodeling of the precursors of the sensory epithelium to achieve an extended array of HCs along the tonotopic axis. Since the complete population of PrCs is present by E14, well before the cochlear duct reaches its full length, subsequent rearrangements of that population must occur. Although previous studies have hypothesized roles for cell movements as a result of both RI and CE, direct visualization of these processes had not been reported.

To better characterize the factors that regulate cochlear extension, changes in cell size and distribution were measured for PrCs, HCs and SCs at E14, E16 and P0 (Fig. 1). Results indicate that an initially pseudostratified population of PrCs extends along the base-to-apex axis through a combination of cellular rearrangement and increased cell volume (Fig. 6). Cellular rearrangements, which are biased along the axis of extension, lead to decreases in both the density and stratification of PrCs. In addition, the volumes of developing HCs and SCs increase between E14 and P0, providing another mechanism for extension. To determine whether the combined effects of cellular rearrangements and growth are sufficient to account for the overall outgrowth of the prosensory domain/OC between E14 and P0, we modeled the contributions of both processes from E14-E16 and E16-P0 (Fig. S5). The results indicate an extension of ~320% between E14 and P0. Direct measurement of cochlear extension between the same time points indicates an increase of ~220%. The basis for the differences in these values is not clear; however, cell size is heterogeneous along the base-to-apex

Development (2017) 144, 3766-3776 doi:10.1242/dev.151761

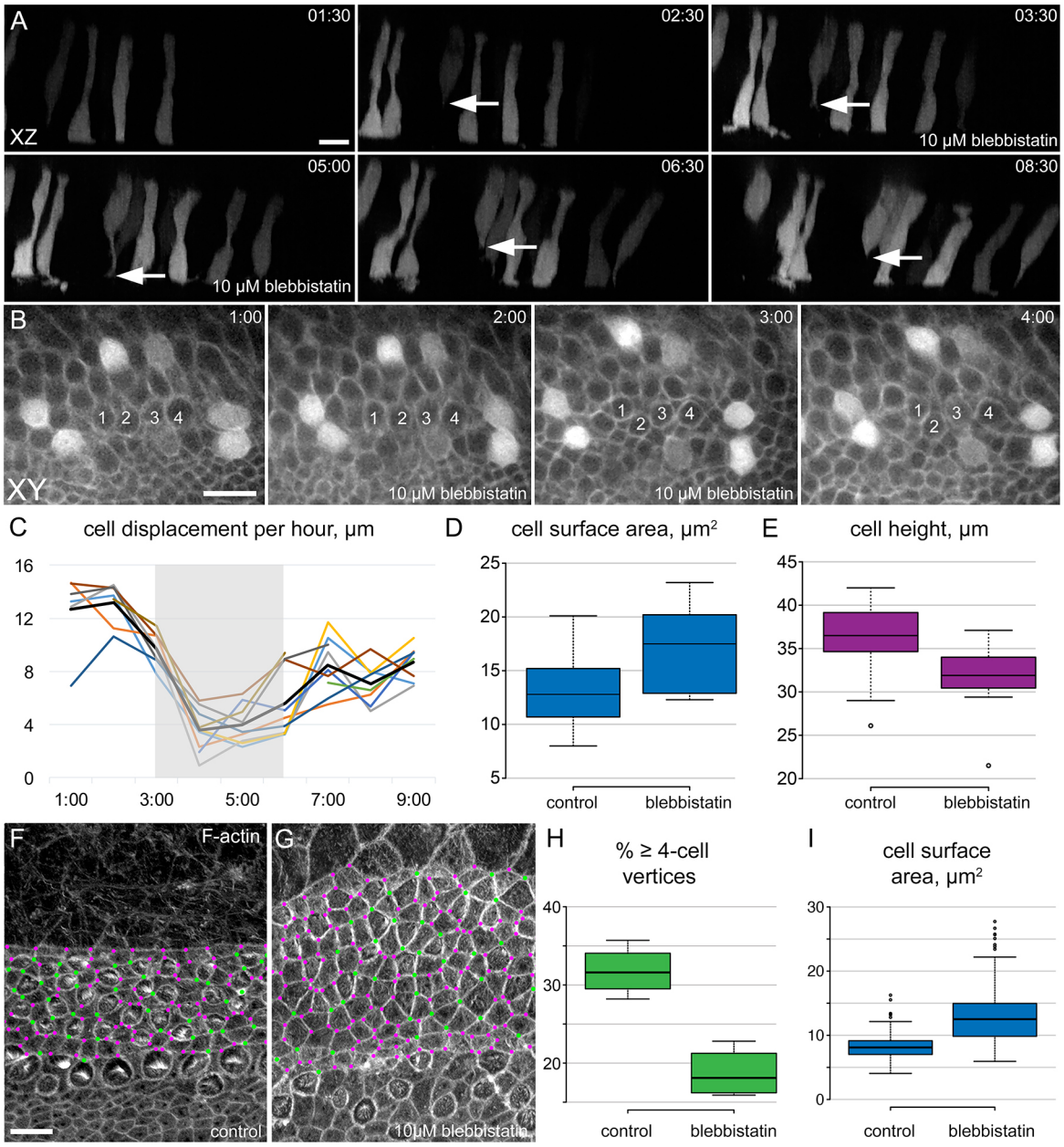

Fig. 5. MyoII is required for cell migration and intercalation. (A) *xz* projections from a time-lapse (Movie 6) of a tdTomato-labeled E15 explant treated with blebbistatin for 3 h. During MyoII inhibition, a presumptive HC extends a basal protrusion (arrows), which retracts when blebbistatin is diluted. Scale bar: 10 μm. (B) Time-lapse images from an *Atoh1*^{Cre*PR}; *R26R*$^{tdTomato/mT-mG}$ E16 explant labeled with membrane tdTomato and Cre-induced cytoplasmic tdTomato. Blebbistatin (10 μM) slows cell movement and disrupts cellular organization. Four putative HCs (numbered) become misaligned during MyoII inhibition. See Movie 7. Scale bar: 10 μm. (C) Cell displacement per hour in blebbistatin-treated explants. Each line represents the displacement of a single cell. The gray box indicates the duration of the 10 μM blebbistatin treatment. After 3 h, blebbistatin was diluted to 1 μM, and the rate of cell movement gradually increased. (D) Measurements of luminal surface area of PrCs from time-lapse sequences, showing an increase in surface area before and after 2.5 h of 10 μM blebbistatin treatment (P<0.05). (E) Cell height of the PrCs in D, measured along the *z*-axis of *xz* projections, decreases after 2.5 h of MyoII inhibition (P<0.01). (D,E) n=3 explants, 10 cells. (F) Control cochlear explant established at E13 and maintained for 3 DIV, stained with phalloidin. Cell vertices containing three (magenta) or four or more cells (green) are indicated. Scale bar: 10 μm. (G) Similar image as in F from an explant treated with 10 μM blebbistatin, with fewer four-cell vertices. (H) Blebbistatin treatment leads to a decrease in the percentage of vertices containing four or more cells (P<0.001). Number of vertices: 1218, control; 1471, blebbistatin. (I) The luminal surface area of both HCs and SCs increases in response to MyoII inhibition (P<0.001). Number of cells: 133, control; 157, blebbistatin. (H,I) Four explants per condition.

axis of the cochlea. Since our analysis was restricted to the basal region, where cells are larger compared with more apical regions, it is possible that the larger size of both HCs and SCs could cause this overestimation. In addition, we were unable to include the length of the cochlear hook in our calculation of cochlear length, which could cause an underestimation of the total change in length.

The decrease in cell stratification as the cochlea extends is consistent with a process of RI in which pseudostratified PrCs intercalate towards the basement membrane. This process leads to thinning of the epithelium and the generation of positive cellular displacement forces in directions perpendicular to the axis of intercalation. Concomitant with the process of RI, PrCs increase in

Development (2017) 144, 3766-3776 doi:10.1242/dev.151761

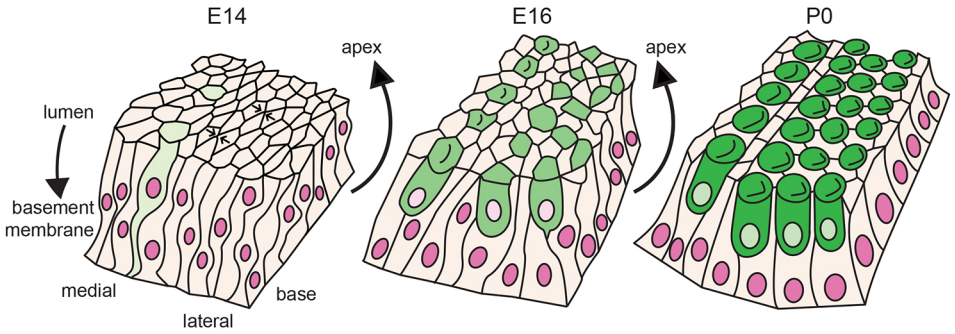

Fig. 6. Model of cell movement and rearrangement of OC cells during cochlear development. At E14, PrCs are highly pseudostratified in a relatively wide array. Cells intercalate at the luminal surface (arrows), and radially intercalate through the basement membrane to luminal axis. Presumptive HCs (light green) have thin protrusions toward the basement membrane, and overall cell movement is towards the apex. At E16, movement toward the apex continues, but differentiating HCs (green) no longer contact the basement membrane. Some four-cell junctions are still present, and stratification of the epithelium has decreased. By P0, cellular patterning is mostly complete, creating the longer, thinner OC with a mosaic of HCs and SCs.

volume, providing further potential displacement forces. While these displacement forces could be equally distributed along both the base-to-apex and medial-lateral axes, their primary effect is extension towards the apex of the cochlea. The net flow of cells towards the apex leads to fewer cells across the medial-lateral width at any particular location along the base-to-apex length. The bias in displacement towards the apex is likely to be mediated, at least in part, by the apically directed migration of PrCs/SCs, but could also be influenced by increased resistance to displacement along the medial-lateral axis in comparison to the base-to-apex axis, and the observed intercalation and convergence along the medial-lateral axis, demonstrated by live imaging between E14 and E16. The somewhat limited role of CE during cochlear elongation is surprising given the defects in cochlear length and patterning in different PCP mutants such as *Vangl2* or *Dvl1/2* (Montcouquiol et al., 2003; Wang et al., 2005). However, recent results have demonstrated a role for both *Vangl2* and *dishevelled* during the RI that occurs during gastrulation and neurulation in *Xenopus* (Ossipova et al., 2015). Considering the results presented here, a closer examination of the effects of PCP mutants on both CE and RI during cochlear development is warranted.

Analysis of individually labeled PrCs/SCs allowed visualization of the migration of these cells for the first time. The basal processes of these cells generate movements that are consistent with active crawling along the basement membrane and the generation and retraction of cellular protrusions is consistent with directed cellular movements. Previous work in the developing neural tube has demonstrated a bias in protrusive activity along the axis of migration (Jayachandran et al., 2016; Voiculescu et al., 2007; Wallingford et al., 2000; Williams et al., 2014; Yen et al., 2009). Protrusive activity in the PrC/SC population was generally oriented at 45° relative to both the axis of extension and the perpendicular axis of convergence. Analysis of productive T1 cell-cell exchanges was similarly oriented at a ∼45° angle relative to the axis of extension, suggesting a complex series of cellular rearrangements that may be a result of both outgrowth and patterning.

As is the case in other systems (Pfister et al., 2016; Simões Sde et al., 2014; Xu et al., 2016), both cellular intercalation at the luminal surface and cellular migration of cell bodies is dependent on MyoII. Previous work had demonstrated inhibition of cochlear cellular intercalation and junctional remodeling in response to either pharmacological or genetic inhibition of MyoII (Yamamoto et al., 2009). However, in contrast to recent reports indicating that inhibition of MyoII results in a significant decrease in the ability of cells to generate protrusions (Rai et al., 2017; Sayyad et al., 2015), cochlear epithelial cells continued to extend protrusions in the presence of blebbistatin. Whether the resulting inhibition of cell migration is a result of the disruption in protrusive bias, or because MyoII also plays a more direct role in generating migratory forces within a cell (Ma and Adelstein, 2014; Newell-Litwa et al., 2015), cannot be determined at this point.

Overall, the results presented here provide a clearer picture of the cellular processes that occur during cochlear outgrowth. Following terminal mitosis, PrCs are organized in a pseudostratified band. As development continues, the cochlear epithelium thins through RI intercalation of the PrC population. This intercalation provides a driving force that acts primarily along the axis of extension. At the same time, PrCs in contact with the basement membrane actively move towards the apex of the cochlea as part of an epibolic migration. Prior to E16, a limited amount of convergence within the prosensory domain is also observed, but a concomitant increase in PrC volume compensates for this convergence, causing the overall width of the epithelium to remain constant between E14 and E16. Cellular intercalations, both RI and CE, largely end at ∼E16, but ongoing increases in cellular volume continue to drive extension of the OC. Multiple aspects of this process are mediated through MyoII-dependent changes in cellular morphology. These results provide the first comprehensive description of the cellular processes that drive the remodeling of the prosensory domain during cochlear development, and suggest that a combination of RI, CE and cellular growth all contribute to cochlear extension along the base-to-apex axis.

MATERIALS AND METHODS

Mice

The following strains were used: *Atoh1*$^{tm5.1(cre/PGR)Hzo}$ [*Atoh1*^{Cre*PR} (Rose et al., 2009)], *Sox2*$^{tm1.1(cre)Jpmb}$ [*Sox2*^{CreERT2} (Arnold et al., 2011)], *Gt(ROSA)26Sor*$^{tm14(CAG-tdTomato)Hze}$ and *Gt(ROSA)26Sor*$^{tm6(CAG-ZsGreen1)Hze}$ [*R26R*^{tdTomato} and *R26R*^{ZsGreen} (Madisen et al., 2010)] and *xGt(ROSA)26Sor*$^{tm4(ACTB-tdTomato,-EGFP)Luo}$ [*R26R*$^{mT-mG}$ (Muzumdar et al., 2007)]. In most cases, male mice carrying a *Cre* allele and homozygous for a fluorescent reporter were mated to CD1 female mice to generate a timed pregnancy. CD1 mice for sections and extension assays were obtained from Charles River. All mice were maintained according to the animal care and use protocols of the NINDS and NIDCD Animal Health and Care Section of the National Institutes of Health.

In vivo labeling

Female CD1 mice from timed matings to *Sox2*^{CreERT2}; *R26R*$^{mT-mG/mT-mG}$ males were given 100-200 µg tamoxifen (Sigma-Aldrich) and 4 mg progesterone (Sigma-Aldrich) by oral gavage at 12.5 days post-coitus to

Development (2017) 144, 3766-3776 doi:10.1242/dev.151761

induce Cre^{ERT2} activity. Embryos were collected at E15, inner ears removed and fixed for 2 h in 4% paraformaldehyde (PFA).

Cochlear explants

Embryos were collected from timed-pregnant females, and cochlear explants were established at E13 to E16 as previously described (Driver et al., 2013). For live imaging, the apicalmost quarter of the cochlear duct was removed prior to culturing. For extension assays, approximately the basal two-thirds of the cochlear duct was explanted with the roof of the duct attached. Cochlear epithelial explants were cultured with attached mesenchyme in DMEM:F12 medium with 10% FBS on Mattek dishes coated with a 1:15 dilution of Matrigel (Corning). To induce Cre activity, explants were treated with mifepristone (RU486, Sigma-Aldrich) or 4-hydroxytamoxifen (4OH-tamoxifen, Sigma-Aldrich) to achieve scattered fluorescent reporter expression (Table 1).

For live imaging of the luminal surface of the cochlear epithelium, explants were established similarly, but diluted Matrigel was applied to a polycarbonate filter (Sterlitech) and explants were cultured on floating filters at the air-liquid interface (see live imaging below).

Immunofluorescence

To visualize OC cells during cochlear development, inner ears from CD1 mice were collected at E14, E16 or P0 and fixed for 2 h in 4% PFA. Overlapping expression of CDKN1B (rabbit polyclonal, 1:500, NeoMarkers, RB-9019-P1, RRID:AB_149788) and SOX2 (goat polyclonal, 1:300, Santa Cruz Biotechnology, sc-17320, RRID: AB_2286684) was used to examine changes in the distribution of PrCs. Cochlear explants were fixed for 20-30 min in 4% PFA, then processed similarly. Other primary antibodies used were chicken polyclonal anti-GFP (1:1000, Aves Labs, GFP-1010, RRID:AB_10000240), mouse monoclonal anti-Pou4f3 (1:200, Santa Cruz Biotechnology, sc-81980, RRID: AB_2167543) and rabbit polyclonal anti-myosin VIIa (1:2000, Proteus Biosciences, 25-6790, RRID:AB_10015251). Secondary antibodies (1:1000) and Alexa Fluor-labeled phalloidin were from ThermoFisher Scientific. For analysis of changes in cellular distribution and volume, whole mounts were imaged on a Zeiss LSM 710 confocal microscope and analyzed using Zen Black software (Zeiss).

Live imaging

Four-dimensional time-lapse images were collected using either an inverted Axiovision Zeiss spinning disk confocal microscope with an EMCCD camera, or on an inverted PerkinElmer UltraVIEW Time Lapse Image Analysis System with either an EMCCD or sCMOS camera. *z*-stacks, usually with a 0.5 µm step, were collected at 3, 5 or 10 min intervals for up to 16 h. For velocity and CE measurements, images were captured with a 40×1.4 NA or 63×1.4 NA oil-immersion objective at either 512×512 pixels (EMCCD) or 672×512 pixels (sCMOS). For protrusion analysis, images were captured with the 63× objective. To inhibit MyoII activity, blebbistatin (Sigma-Aldrich) in DMSO was added to cultures to a final concentration of 10 µM, and 'washout' was dilution of blebbistatin to 1 µM. To image the luminal surface of the epithelium, polycarbonate filters with attached explants were inverted and submerged in Mattek dishes so that the luminal surface of the epithelium was closest to the coverslip. The filters were stabilized with a short piece of tungsten wire. Images were collected from these explants for a maximum of 6 h.

Image analysis

Post-processing of time-lapse images was carried out using Volocity software (PerkinElmer). Typically, image processing included background subtraction, iterative deconvolution with calculated point spread functions, rotating to align the elongation axis as close to horizontal as possible, and noise reduction. Cell tracking was performed by thresholding and object identification in Volocity, and used to generate measurements for displacement rate, straightness index, and cell centroid locations. For the CE analysis in Fig. 3, the relative distances between cell pairs initially less than 50 µm apart along the base-to-apex (x) axis were determined at the 2 h and 8 h time points. This 6 h interval was used because the cells of analyzed cell pairs both remained within the frame during that time.

T1 neighbor exchange nematics were calculated using TissueMiner software (Etournay et al., 2016). Time-lapse sequences of membrane-associated tdTomato from the luminal surface of E15 $R26R^{mT\text{-}mG}$ explants were segmented with Tissue Analyzer in ImageJ (Aigouy et al., 2016), hand corrected and verified, then processed through the automated workflow in TissueMiner.

Protrusion analysis was conducted using the CellGeo software package (Tsygankov et al., 2014), running in MATLAB (MathWorks). Time-lapse images of maximum-intensity *z*-stack projections of fluorescently labeled cells sufficiently distant from other labeled cells were cropped to contain a single cell within the frame. Cell movement was first subtracted using a custom ImageJ plug-in and centroid coordinates generated in Volocity. Cell protrusions were then identified, measured, and tracked in CellGeo. Protrusions were identified with a maximum width of 1.25 µm and a minimum length of 1.9 µm.

Table 1. Genotype and *in vitro* induction parameters for reporter lines

Cre	Reporter	Treatment
$Atoh1^{Cre*PR}$	$R26R^{tdTomato}$ or $R26R^{ZsGreen}$	1 nM RU486, 1 h
$Atoh1^{Cre*PR}$	$R26R^{mT\text{-}mG}$	10 nM RU486, 16 h
$Sox2^{CreERT2}$	$R26R^{tdTomato}$ or $R26R^{ZsGreen}$	1 nM 4OH-tamoxifen, 1 h
$Sox2^{CreERT2}$	$R26R^{mT\text{-}mG}$	2 nM 4OH-tamoxifen, 16 h

Statistical analysis

For all box plots presented in figures, the center lines show median values, box limits indicate the 25th and 75th percentiles, whiskers extend 1.5 times the interquartile range from the 25th and 75th percentiles, and outliers are represented by dots. Box plots were generated using the BoxPlotR online tool (Spitzer et al., 2014). For bar charts, data are presented as mean±s.e.m. Statistically significant differences among multiple measurements were determined by one-way ANOVA followed by Tukey's HSD test. Statistical differences between two values were determined by two-tailed Student's *t*-test. Angular distributions were determined to be non-uniform by χ^2 test, and comparisons of two angular distributions were made by the Watson-Wheeler test.

Acknowledgements

We thank Dr Joseph Burns (Decibel Therapeutics) for assistance with Fiji; Dr Denis Tsygankov (Georgia Tech) for assistance with CellGeo; Dr Zoë Mann (University College London) for help with preliminary live imaging experiments; Dr Thomas Coate (Georgetown University), Dr Katie Kindt and Dr Michael Kelly (NIDCD) for critical comments on the manuscript.

Competing interests

The authors declare no competing or financial interests.

Author contributions

Conceptualization: E.C.D., M.W.K.; Methodology: E.C.D., M.W.K.; Formal analysis: E.C.D., M.W.K.; Investigation: E.C.D., A.N., M.W.K.; Writing - original draft: E.C.D., M.W.K.; Writing - review & editing: E.C.D., M.W.K.; Visualization: E.C.D., M.W.K.; Funding acquisition: M.W.K.

Funding

This work was supported by funds from the Division of Intramural Research of the National Institute on Deafness and Other Communication Disorders, National Institutes of Health (DC000059). Deposited in PMC for release after 12 months.

Supplementary information

Supplementary information available online at
http://dev.biologists.org/lookup/doi/10.1242/dev.151761.supplemental

References

Aigouy, B., Umetsu, D. and Eaton, S. (2016). Segmentation and quantitative analysis of epithelial tissues. *Methods Mol. Biol.* **1478**, 227-239.

Arnold, K., Sarkar, A., Yram, M. A., Polo, J. M., Bronson, R., Sengupta, S., Seandel, M., Geijsen, N. and Hochedlinger, K. (2011). Sox2(+) adult stem and progenitor cells are important for tissue regeneration and survival of mice. *Cell Stem Cell* **9**, 317-329.

Development (2017) 144, 3766-3776 doi:10.1242/dev.151761

Bertet, C., Sulak, L. and Lecuit, T. (2004). Myosin-dependent junction remodelling controls planar cell intercalation and axis elongation. *Nature* **429**, 667-671.

Blankenship, J. T., Backovic, S. T., Sanny, J. S. P., Weitz, O. and Zallen, J. A. (2006). Multicellular rosette formation links planar cell polarity to tissue morphogenesis. *Dev. Cell* **11**, 459-470.

Burda, H. and Branis, M. (1988). Postnatal development of the organ of Corti in the wild house mouse, laboratory mouse, and their hybrid. *Hear. Res.* **36**, 97-105.

Chacon-Heszele, M. F., Ren, D., Reynolds, A. B., Chi, F. and Chen, P. (2012). Regulation of cochlear convergent extension by the vertebrate planar cell polarity pathway is dependent on p120-catenin. *Development* **139**, 968-978.

Chen, P. and Segil, N. (1999). p27(Kip1) links cell proliferation to morphogenesis in the developing organ of Corti. *Development* **126**, 1581-1590.

Chen, P., Johnson, J. E., Zoghbi, H. Y. and Segil, N. (2002). The role of Math1 in inner ear development: uncoupling the establishment of the sensory primordium from hair cell fate determination. *Development* **129**, 2495-2505.

Driver, E. C., Sillers, L., Coate, T. M., Rose, M. F. and Kelley, M. W. (2013). The Atoh1-lineage gives rise to hair cells and supporting cells within the mammalian cochlea. *Dev. Biol.* **376**, 86-98.

Ebrahim, S., Fujita, T., Millis, B. A., Kozin, E., Ma, X., Kawamoto, S., Baird, M. A., Davidson, M., Yonemura, S., Hisa, Y. et al. (2013). NMII forms a contractile transcellular sarcomeric network to regulate apical cell junctions and tissue geometry. *Curr. Biol.* **23**, 731-736.

Elul, T. and Keller, R. (2000). Monopolar protrusive activity: a new morphogenic cell behavior in the neural plate dependent on vertical interactions with the mesoderm in Xenopus. *Dev. Biol.* **224**, 3-19.

Etournay, R., Merkel, M., Popović, M., Brandl, H., Dye, N. A., Aigouy, B., Salbreux, G., Eaton, S. and Jülicher, F. (2016). TissueMiner: a multiscale analysis toolkit to quantify how cellular processes create tissue dynamics. *eLife* **5**, e14334.

Jayachandran, P., Olmo, V. N., Sanchez, S. P., McFarland, R. J., Vital, E., Werner, J. M., Hong, E., Sanchez-Alberola, N., Molodstov, A. and Brewster, R. M. (2016). Microtubule-associated protein 1b is required for shaping the neural tube. *Neural Dev.* **11**, 1.

Kiernan, A. E. (2013). Notch signaling during cell fate determination in the inner ear. *Semin. Cell Dev. Biol.* **24**, 470-479.

Kiernan, A. E., Pelling, A. L., Leung, K. K. H., Tang, A. S. P., Bell, D. M., Tease, C., Lovell-Badge, R., Steel, K. P. and Cheah, K. S. E. (2005). Sox2 is required for sensory organ development in the mammalian inner ear. *Nature* **434**, 1031-1035.

Ma, X. and Adelstein, R. S. (2014). The role of vertebrate nonmuscle Myosin II in development and human disease. *Bioarchitecture* **4**, 88-102.

Madisen, L., Zwingman, T. A., Sunkin, S. M., Oh, S. W., Zariwala, H. A., Gu, H., Ng, L. L., Palmiter, R. D., Hawrylycz, M. J., Jones, A. R. et al. (2010). A robust and high-throughput Cre reporting and characterization system for the whole mouse brain. *Nat. Neurosci.* **13**, 133-140.

Mann, Z. F. and Kelley, M. W. (2011). Development of tonotopy in the auditory periphery. *Hear. Res.* **276**, 2-15.

McKenzie, E., Krupin, A. and Kelley, M. W. (2004). Cellular growth and rearrangement during the development of the mammalian organ of Corti. *Dev. Dyn.* **229**, 802-812.

Montcouquiol, M., Rachel, R. A., Lanford, P. J., Copeland, N. G., Jenkins, N. A. and Kelley, M. W. (2003). Identification of Vangl2 and Scrb1 as planar polarity genes in mammals. *Nature* **423**, 173-177.

Mu, M. Y., Chardin, S., Avan, P. and Romand, R. (1997). Ontogenesis of rat cochlea. A quantitative study of the organ of Corti. *Brain Res. Dev. Brain Res.* **99**, 29-37.

Muzumdar, M. D., Tasic, B., Miyamichi, K., Li, L. and Luo, L. (2007). A global double-fluorescent Cre reporter mouse. *Genesis* **45**, 593-605.

Newell-Litwa, K. A., Horwitz, R. and Lamers, M. L. (2015). Non-muscle myosin II in disease: mechanisms and therapeutic opportunities. *Dis. Model. Mech.* **8**, 1495-1515.

Ossipova, O., Chu, C.-W., Fillatre, J., Brott, B. K., Itoh, K. and Sokol, S. Y. (2015). The involvement of PCP proteins in radial cell intercalations during Xenopus embryonic development. *Dev. Biol.* **408**, 316-327.

Ou, H. C., Bohne, B. A. and Harding, G. W. (2000). Noise damage in the C57BL/CBA mouse cochlea. *Hear. Res.* **145**, 111-122.

Pfister, K., Shook, D. R., Chang, C., Keller, R. and Skoglund, P. (2016). Molecular model for force production and transmission during vertebrate gastrulation. *Development* **143**, 715-727.

Rai, V., Thomas, D. G., Beach, J. R. and Egelhoff, T. T. (2017). Myosin IIA heavy chain phosphorylation mediates adhesion maturation and protrusion in three dimensions. *J. Biol. Chem.* **292**, 3099-3111.

Rose, M. F., Ahmad, K. A., Thaller, C. and Zoghbi, H. Y. (2009). Excitatory neurons of the proprioceptive, interoceptive, and arousal hindbrain networks share a developmental requirement for Math1. *Proc. Natl. Acad. Sci. USA* **106**, 22462-22467.

Rozbicki, E., Chuai, M., Karjalainen, A. I., Song, F., Sang, H. M., Martin, R., Knölker, H.-J., MacDonald, M. P. and Weijer, C. J. (2015). Myosin-II-mediated cell shape changes and cell intercalation contribute to primitive streak formation. *Nat. Cell Biol.* **17**, 397-408.

Ruben, R. J. (1967). Development of the inner ear of the mouse: a radioautographic study of terminal mitoses. *Acta Otolaryngol. Suppl.* **220**, 1-44.

Sayyad, W. A., Amin, L., Fabris, P., Ercolini, E. and Torre, V. (2015). The role of myosin-II in force generation of DRG filopodia and lamellipodia. *Sci. Rep.* **5**, 7842.

Simões Sde, M., Mainieri, A. and Zallen, J. A. (2014). Rho GTPase and Shroom direct planar polarized actomyosin contractility during convergent extension. *J. Cell Biol.* **204**, 575-589.

Spitzer, M., Wildenhain, J., Rappsilber, J. and Tyers, M. (2014). BoxPlotR: a web tool for generation of box plots. *Nat. Methods* **11**, 121-122.

Tada, M. and Heisenberg, C.-P. (2012). Convergent extension: using collective cell migration and cell intercalation to shape embryos. *Development* **139**, 3897-3904.

Tsygankov, D., Bilancia, C. G., Vitriol, E. A., Hahn, K. M., Peifer, M. and Elston, T. C. (2014). CellGeo: a computational platform for the analysis of shape changes in cells with complex geometries. *J. Cell Biol.* **204**, 443-460.

Voiculescu, O., Bertocchini, F., Wolpert, L., Keller, R. E. and Stern, C. D. (2007). The amniote primitive streak is defined by epithelial cell intercalation before gastrulation. *Nature* **449**, 1049-1052.

Wallingford, J. B., Rowning, B. A., Vogeli, K. M., Rothbächer, U., Fraser, S. E. and Harland, R. M. (2000). Dishevelled controls cell polarity during Xenopus gastrulation. *Nature* **405**, 81-85.

Wang, J., Mark, S., Zhang, X., Qian, D., Yoo, S.-J., Radde-Gallwitz, K., Zhang, Y., Lin, X., Collazo, A., Wynshaw-Boris, A. et al. (2005). Regulation of polarized extension and planar cell polarity in the cochlea by the vertebrate PCP pathway. *Nat. Genet.* **37**, 980-985.

Wang, J., Hamblet, N. S., Mark, S., Dickinson, M. E., Brinkman, B. C., Segil, N., Fraser, S. E., Chen, P., Wallingford, J. B. and Wynshaw-Boris, A. (2006). Dishevelled genes mediate a conserved mammalian PCP pathway to regulate convergent extension during neurulation. *Development* **133**, 1767-1778.

Williams, M., Yen, W., Lu, X. and Sutherland, A. (2014). Distinct apical and basolateral mechanisms drive planar cell polarity-dependent convergent extension of the mouse neural plate. *Dev. Cell* **29**, 34-46.

Xu, B., Washington, A. M., Domeniconi, R. F., Ferreira Souza, A. C., Lu, X., Sutherland, A. and Hinton, B. T. (2016). Protein tyrosine kinase 7 is essential for tubular morphogenesis of the Wolffian duct. *Dev. Biol.* **412**, 219-233.

Yamamoto, N., Okano, T., Ma, X., Adelstein, R. S. and Kelley, M. W. (2009). Myosin II regulates extension, growth and patterning in the mammalian cochlear duct. *Development* **136**, 1977-1986.

Yen, W. W., Williams, M., Periasamy, A., Conaway, M., Burdsal, C., Keller, R., Lu, X. and Sutherland, A. (2009). PTK7 is essential for polarized cell motility and convergent extension during mouse gastrulation. *Development* **136**, 2039-2048.